REPORT DOCUMENTATION PAGE

AFRL-SR-AR-TR-03-

0251

1. AGENCY USE ONLY *(Leave blank)*	2. REPORT DATE	3. REPOR...
		01 MAY 2002 - 30 APR 2003 Final Report

4. TITLE AND SUBTITLE
(DURIP FY02) X-Ray Powder Diffractometer as a Structural toll for the development of Semiconducting Inorganic-Organic Composite Chalcogenides as efficient Thermoelectric Materials

5. FUNDING NUMBERS
61103D
3484/US

6. AUTHOR(S)
Dr Feng

7. PERFORMING ORGANIZATION NAME(S) AND ADDRESS(ES)
UNIVERSITY OF CALIFORNIA
200 UNIVERSITY OFFICE BLDG
RIVERSIDE CA 92521

8. PERFORMING ORGANIZATION REPORT NUMBER

9. SPONSORING/MONITORING AGENCY NAME(S) AND ADDRESS(ES)
AFOSR/NE
4015 WILSON BLVD
SUITE 713
ARLINGTON VA 22203

10. SPONSORING/MONITORING AGENCY REPORT NUMBER
F49620-02-1-0238

11. SUPPLEMENTARY NOTES

12a. DISTRIBUTION AVAILABILITY STATEMENT
APPROVED FOR PUBLIC RELEASE, DISTRIBUTION UNLIMITED

12b. DISTRIBUTION CODE

13. ABSTRACT *(Maximum 200 words)*

With the support of AFOSR-DURIP, an X-ray powder Diffractometer (model: Bruker D8 Advance theta/theta system) has been purchased, installed and put into use now. The instrument has brought great impact iii both research and education on campus. A large number of new materials has been synthesized and characterized with the newly installed instrument. The properties of these new compounds as efficient thermoelectric materials are currently being evaluated. Synthetic, structural, and preliminary property descriptions of these novel materials have been reported in publications acknowledging the support of AFOSR-DURIP. A summary of research and educational activities, major finding, and the plan of current and future uses of the instrument is given here.

20030731 049

14. SUBJECT TERMS			15. NUMBER OF PAGES / 16. PRICE CODE
17. SECURITY CLASSIFICATION OF REPORT	18. SECURITY CLASSIFICATION OF THIS PAGE	19. SECURITY CLASSIFICATION OF ABSTRACT	20. LIMITATION OF ABSTRACT
UNCLASSIFIED	UNCLASSIFIED	UNCLASSIFIED	UL

NE

Final Report

AFOSR DURIP Grant: F49620-02-1-0238

X-ray Powder Diffractometer as a Structural Tool for the Development of Semiconducting Inorganic-Organic Composite Chalcogenides as Efficient Thermoelectric Materials

Principal Investigator: Pingyun Feng

Department of Chemistry, University of California at Riverside
Riverside, CA 92521

Abstract: With the support of AFOSR-DURIP, an X-ray powder Diffractometer (model: Bruker D8 Advance theta/theta system) has been purchased, installed and put into use now. The instrument has brought great impact in both research and education on campus. A large number of new materials has been synthesized and characterized with the newly installed instrument. The properties of these new compounds as efficient thermoelectric materials are currently being evaluated. Synthetic, structural, and preliminary property descriptions of these novel materials have been reported in publications acknowledging the support of AFOSR-DURIP. A summary of research and educational activities, major finding, and the plan of current and future uses of the instrument is given here.

Publications Acknowledging the Support of AFOSR-DURIP

"Microporous and Photoluminescent Chalcogenide Zeolite Analogs" Zheng, N.; Bu, X.; Wang, B.; Feng*, P. *Science* **2002**, 298, 2366-2369.

"Templated Assembly of Sulfide Nanoclusters into Cubic-C_3N_4 Type Framework" Bu, X.; Zheng, N.; Li, Y.; Feng*, P. *J. Am. Chem. Soc.* **2003**, 125, 6024-6025.

"Nonaqueous Synthesis and Selective Crystallization of Gallium Sulfide Clusters into Three-Dimensional Photoluminesce supperlattices" Zheng, N.; Bu, X.; Feng*, P. *J. Am. Chem. Soc.* **2003**, *125, 1138-1139.*

I. Research and Educational Activities

(a) Research Activities

The goal of the project was to integrates synthesis and characterization to develop efficient thermoelectric materials based on heavy chalcogenides inorganic–organic composite materials. The strategy is to synthesize new materials with well-ordered inorganic framework and disordered organic species in the channel or cages of the inorganic network. Disordered organic guest materials are expected to reduce the lattice thermal conductivity and the ordered inorganic framework will maintain the electronic conductivity. Low thermal conductivity and high electronic conductivity are two essential requirements for efficient thermoelectric materials.

Syntheses

The research activities include the exploratory synthesis of novel chalcogenides via hydro- or solvo-thermal synthesis under low temperature conditions (<200°C). Such synthesis conditions help to develop porous materials or other open framework materials that are usually metastable and could not be made at higher temperatures.

The synthetic efforts focus on exploring various compositional domains. In general, we start with the phase domain consisting of trivalent metal chalcogenides. With the knowledge obtained from these binary systems. We move on to more complex ternary systems by incorporating mono-, di-, or tetra-valent cations (such as Cu^{+}, Zn^{2+}, Mn^{2+}, Ge^{4+}, Sn^{4+}). These ternary systems are expected to have more flexibility on framework charges and configurations. From the experimental results we have obtained so far, in order to synthesize larger clusters and more open framework materials, lower charged metal cations are required to charge-balance S^{2-}, and Se^{2-} anions at the core of chalcogenide clusters.

With each compositional domain, we also examine effects of various synthetic parameters on the structures and properties of the resulting materials. These synthetic parameters include temperature, pH, starting materials, solvents, and nature of charge-balancing structure-directing agents. These materials are systematically screened by x-ray diffractometer acquired with the support of the AFOSR-DURIP. Many new phases are identified. For these new phases, we focus on the transport property measurement and detailed structural characterization with the goal of understanding their physical properties in relation to their chemical compositions and crystal structures.

One efficient way for structural and property characterization is to grow single crystal of adequate quality and size for structural characterizations and to prepare samples of adequate purity for property characterizations. The knowledge of structures and properties allows experimental conditions to be systematically varied to identify optimum synthesis conditions for the synthesis of desired materials.

Structures of Crystalline Materials

All crystalline samples are screened routinely with X-ray powder diffraction for identification of phases and for evaluation of sample purity. For unknown samples, single

crystal X-ray diffractions are performed to determine crystal structures. The stability of the materials are investigated by our high temperature apparatus that is attached to our x-ray diffractometer. With this attachment both temperature and environment can be controlled. During the one-year period, we have synthesized a number of new compounds and performed crystal structure determination on several dozens of crystalline materials.

Studies of Physical Properties

For novel materials, we have performed extensive studies on their properties. Chemical compositions are determined and confirmed via a number of different techniques using electron-probe microanalysis, energy dispersive X-ray analysis, and inductively coupled plasma spectroscopy. We have also examined photoluminescent properties, ion-exchange properties, and gas adsorption properties. The thermal stability of these materials is studied using thermal gravimetric analysis, differential thermal analysis, and temperature-dependent X-ray powder analysis. Very recently, we have also started to investigate the transport property of these materials. With the recent installation of the new PPMS (Physical Property Measurement System) on campus, our research will be greatly facilitated. The thermoelectric properties measurements are currently performed in collaboration with Prof. Galen Stucky's laboratory at University of California at Santa Barbara. The electronic and ionic conductivity under different temperatures and environment are being studied in my lab using impedance spectroscopy. Some detailed results are given below in the Major Finding section.

(b) Educational Activities

About 10 students and postdoctors have been trained so far on the use of the diffractometer. The number is expected to increase significantly next academic year with the newly installed high temperature and solid-state detector attachments. The instrument has been and will be used as an educational tool for the training of the x-ray diffraction to a number of undergraduate students, graduate students and postdoctors. In the coming summer, a group of high school students and teachers will be on campus for the outreach materials research program. It is expected that they will synthesize materials by themselves and characterize these materials using this x-ray diffractometer and other instruments on campus. By doing so, these students will have the opportunities to be trained not only in the materials synthesis, but also in the characterization of structural properties and other physical properties.

The diffractometer is open to the whole campus and outside industrial community. A number of students from engineering departments have used the instrument for their materials characterization and a local industrial laboratory is also a regular user of this instrument.

II. Major Findings:

Our research activities in the past year have resulted in major synthetic breakthroughs in the development of organically templated chalcogenide materials. These

research activities have resulted in a number of publications in journals such as *Science* and *J. Am. Chem. Soc.* In addition, the supported instrument has helped led to a new research direction in the area of solid electrolytes and has fostered the research collaboration between our group and several others. The preliminary result on solid electrolytes is currently under review for publication in *Nature*.

Microporous and Photoluminescent Chalcogenide Zeolite Analogs

We synthesized a large family of chalcogenide zeolite analogs by simultaneous triple substitutions of O^{2-} with S^{2-} or Se^{2-}, Si^{4+} with Ge^{4+} or Sn^{4+}, and Al^{3+} with Ga^{3+} or In^{3+}. All four possible M^{4+}/M^{3+} combinations (Ga/Ge, Ga/Sn, In/Ge, and In/Sn) could be realized resulting in four zeolite-type topologies. More than a dozen distinct framework materials have been synthesized by changing either the topological types or the framework composition (Table 1). In addition, new structures can be readily made by replacing organic components with inorganic cations through ion exchange.

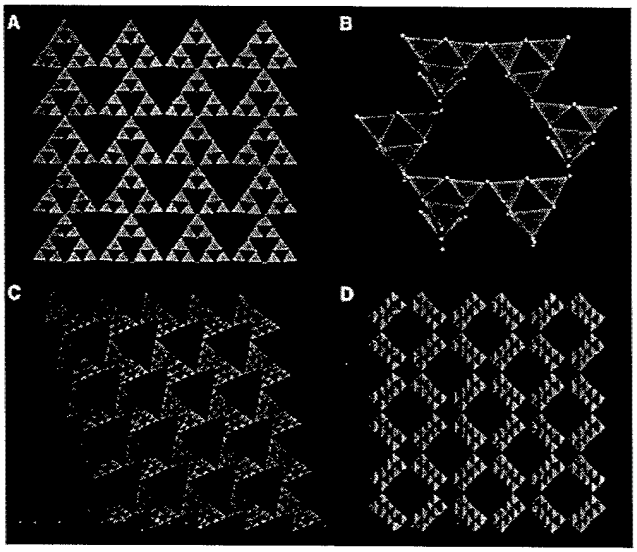

Fig. 1 (A) The 3D M_4X_{10} decorated sodalite framework in UCR-20. (B) Six M_4X_{10} clusters are joined into a 6-membered ring in UCR-21 with the decorated cubic ZnS framework. (C) The 3D framework of UCR-22 with the cubic ZnS type topology decorated with the core-less T4 cluster ($M_{16}X_{34}$). Only one set of lattice in UCR-22 is shown. (D) The 3D framework of UCR-23 with the decorated CrB_4 topology projected down the 16-ring channels.

Based on the structural type, these materials are classified into four families denoted as UCR-20, -21, -22, and –23 (Fig. 1). Each number refers to a series of materials with the same framework topology, but with different chemical compositions in either framework or extra-framework components. For example, UCR-20 can be made in all four M^{4+}/M^{3+} combinations, giving rise to four sub-families denoted as UCR-20GaGeS, UCR-20GaSnS, UCR-20InGeS, and UCR-20InSnS. An individual compound is specified when both the framework composition and the type of extra-framework species are specified (e.g., UCR-20GaGeS-AEP).

One of the most significant progresses demonstrated in this work is the unprecedented and diverse framework compositions. The large variety of chemical compositions makes it possible to tune physical properties such as bandgap, luminescence, pore size, surface area, ion exchange, and chemical stability. Compared to other open framework chalcogenides such as germanium or indium sulfides, these chemical systems are particularly intriguing because of their more direct relationship to aluminosilicate zeolites in both compositions and structures. In some of these materials

that have the unusually low M^{4+} to M^{3+} ratios near 0.20, a very large negative charge develops on the framework that should be desirable in applications such as gas separation and ion exchange, where a high concentration of charge-balancing cations is beneficial.

The extra-large pore size and 3-rings are two other striking features. UCR-22 and UCR-23 have an uncommon pore size consisting of 24 and 16 T-atoms respectively whereas UCR-20 and UCR-21 are both large pore (12 T-atoms) materials. These inorganic frameworks are strictly 4-connected 3D networks commonly used for the systematic description of zeolite frameworks. Unlike known zeolite structure types, a key structural feature is the presence of the adamantane-cage shaped building unit, M_4S_{10}. The M_4S_{10} unit consists of four 3-rings (three T-atoms in a ring) fused together. The presence of 3-rings is one of the most desirable features in a zeolite-type topology because it helps to generate low-density framework.

Although these new chalcogenides are strictly zeolite-type tetrahedral frameworks, it is possible to view them as decoration of even simpler tetrahedral frameworks. Decoration means the replacement of a single atom by a multi-atom cluster having the same connectivity pattern. Here, each M_4S_{10} unit can be treated as a large artificial tetrahedral atom. With this description, UCR-20 has the decorated sodalite-type structure, in which a tetrahedral site in a regular sodalite net is replaced with a M_4S_{10} unit. UCR-21 has the decorated cubic ZnS type structure. UCR-23 has the decorated CrB_4 type network in which tetrahedral boron sites are replaced with M_4S_{10} units.

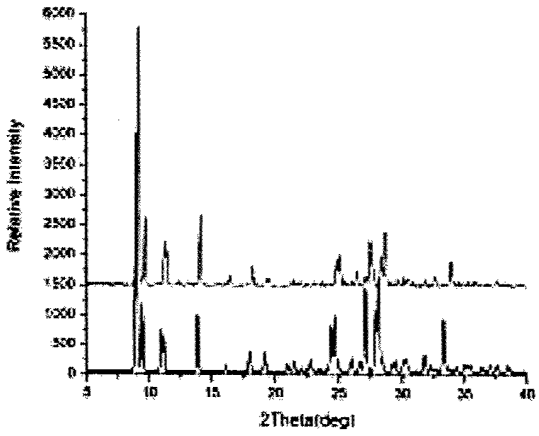

Fig. 2 X-ray powder diffraction spectra of the NH_4^+ exchanged UCR-20GaGeS-TAEA before (bottom) and after (top) calcination.

The new M^{4+}/M^{3+} sulfides reported have significantly improved thermal and mechanical stability over many previously reported crystalline open framework sulfides such as indium sulfides. Selected samples such as UCR-20GaGeS-AEP, UCR-20GaGeS-TAEA, UCR-20InGeS-TMDP, UCR-20InSnS-TMDP, UCR-21GaGeS-AEM, UCR-22InGeS-AEP, UCR-22GaSnS-AEP, and UCR-23GaGeS-AEM maintained their structural and mechanical integrity when heated in air at 300°C for 1hour. In all cases, despite a significant weight loss of up to about 20%, the single-crystal quality is retained as demonstrated by single crystal X-ray diffraction. Powder X-ray diffraction shows that some of these compounds (for example, UCR-20GaGeS-TAEA) are stable at 380°C in argon. A higher thermal stability (at least to 420°C) is observed for the Cs^+ exchanged UCR-20GeS-TAEA under vacuum.

Direct calcination of as-synthesized samples can remove a significant fraction of extra-framework organic components. In one experiment, about 77% of nitrogen and 81% of hydrogen were removed from UCR-20GaGeS-TAEA by direct calcination at 350°C in nitrogen. However, the coke formation makes the removal of carbon more difficult. About 39% of carbon atoms were removed from UCR-20GaGeS-TAEA in the same experiment. Another approach, ion exchange followed by calcination, has been found to be easier for the removal of extra-framework species (Fig. 2).

These new materials undergo ion exchange with many monovalent and divalent metal cations. For example, upon exchange with Cs^+ ions, the percentage of C, H, and N in UCR-20GaGeS-TAEA was dramatically reduced. Yet, the exchanged sample remains highly crystalline as the original sample. The Cs^+ exchanged UCR-20GaGeS-TAEA exhibits the Type I isotherm characteristic of a microporous solid. This sample has a high BET surface area of $807m^2/g$ and a micropore volume of $0.23cm^3/g$ despite the presence of much heavier elements (Cs-Ga-Ge-S) compared to aluminosilicate zeolites.

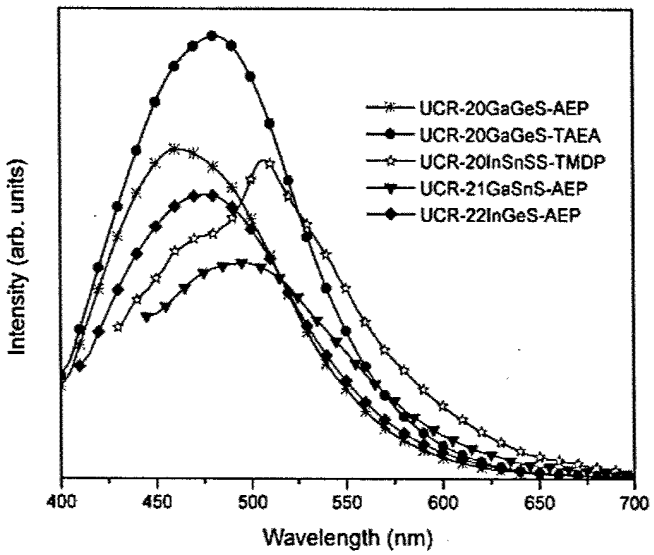

Fig. 3 Photoluminescent emission spectra of some selected compounds.

These new sulfides are also strongly photoluminescent and can be excited with wavelengths from 360 to 420nm. The emission maximum occurs in the range from 460 to 508nm (Fig. 3). For example, UCR-20GaGeS-TAEA strongly luminesces at 480nm when excited at 370nm. The general trend is that materials with heavier elements are excited and luminesce at longer wavelength.

Selective Crystallization of Gallium Sulfide Clusters into Three-Dimensional Superlattices

We have developed a low-temperature, non-aqueous synthesis approach and have successfully prepared a series of gallium sulfide and polysulfide open framework materials built from binary Ga-S and ternary Zn-Ga-S supertetrahedral clusters (Table 2). These novel materials possess unprecedented structural properties and their fluorescent emission wavelength fills the gap between open framework oxides and indium chalcogenides.

All new compounds consist of supertetrahedral clusters that are tetrahedrally shaped fragments of the cubic ZnS type lattice. In the absence of divalent cations, one of the superlattices formed is UCR-7GaS-TETA (Fig. 4) built from T3 ($Ga_{10}S_{18}$) clusters. All four-corners of T3 clusters are shared through S^{2-} bridges. The T3 cluster is known in

both divalent metal thiolates (e.g., $Cd_{10}S_4(SPh)_{16}^{4-}$) and boron or indium sulfides. However, prior to this work, neither the molecular T3 cluster nor its covalent superlattice is known in the Ga-S system.

When divalent cations are introduced either directly through the addition of a salt (e.g. $Zn(NO_3)_2 \cdot 6H_2O$) or through the oxidation of zinc, the reaction system gains an extra capability to form T4 clusters ($Zn_4Ga_{16}S_{33}$), in addition to its inherent ability to form T3 clusters ($Ga_{10}S_{18}$). This is because regular supertetrahedral clusters larger than T3 can only be found in heterometallic compositions. The reason is the local charge balance around the tetrahedrally coordinated sulfur atom in clusters larger than T3. To follow Pauling's electrostatic valence rule, divalent cations are distributed around the tetrahedral S^{2-} site to give a bond valence sum of 2, consistent with the valence of sulfur.

Therefore, both T3 and T4 clusters are likely present in the heterometallic sulfide solution. By using different structure directing agents, one or both of them can be selectively crystallized into a superlattice. In this work, several situations could be distinguished, leading to the synthesis of a number of superlattices built from binary and ternary sulfide clusters.

The first situation involves the use of 1-(2-Aminoethyl)piperazine (AEP) as the structure-directing agent. Only T3 clusters are formed in crystals (denoted as UCR-18GaS-AEP), even if various amounts of zinc are present. An unprecedented feature is the presence of the polysulfide linkage between T3 clusters. This is the first observation of supertetrahedral clusters being linked through polysulfide bonds. Here, T3 clusters are connected at three corners through –S- bridges into a 3-connected sheet with 6-rings (i.e., 6 T3 clusters in a ring). These sheets are joined through –S-S-S- bridges into a 3D framework.

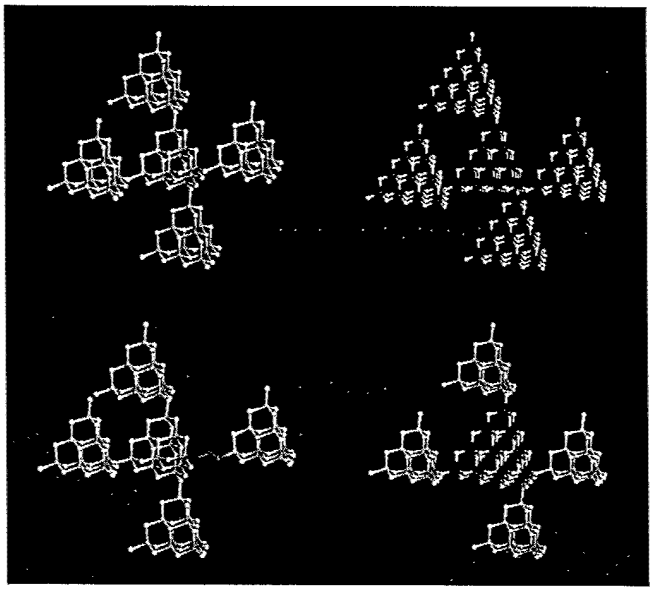

Fig. 4 Four different structure types made from T3 ($Ga_{10}S_{20}$) and T4 ($Zn_4Ga_{16}S_{35}$) clusters. (Top left): the T3-T3 superlattice in UCR-7; (top right): the T4-T4 superlattice in UCR-5; (bottom left): the T3-T3 superlattice through mixed –S- and –S-S-S- bridges in UCR-18; (bottom right): the hybrid T3-T4 superlattice in UCR-19.

The selection of T4 clusters can be achieved with 1,4-bis(3-aminopropyl)piperazine (BAPP). In this case, UCR-5ZnGaS-BAPP (Fig. 4) built from T4 clusters only is formed. Compared to AEP with 9 non-H atoms, BAPP has 14 non-H atoms. The large size of BAPP might be one reason for the preferential selection of large T4 clusters that once crystallize give a larger pore volume.

A very interesting situation occurs when triethylenetetramine (TETA) (10 non-H atoms) is used as structure directing agent. In the absence of Zn^{2+}, it forms a regular T3

($Ga_{10}S_{18}$) superlattice (i.e., UCR-7GaS-TETA). However, when Zn^{2+} cations are introduced to the solution, UCR-19ZnGaS-TETA (Fig. 4) with alternating T3 ($Ga_{10}S_{18}$) and T4 ($Zn_4Ga_{16}S_{33}$) clusters is formed. UCR-19ZnGaS-TETA represents the only superlattice in which two different regular supertetrahedral clusters are joined into a hybrid superlattice. Prior to this work, the T3 cluster is known to connect with the core-less T5 cluster into a superlattice.

Gallium sulfide superlattices reported here serve to bridge a previously observed gap in the emission wavelength of open framework phosphors. It was reported earlier that open-framework oxides have an emission wavelength from 400-440nm. Later, open framework indium sulfides were found to emit in the range from 520 to 570nm. Gallium sulfide superlattices reported here show strong photoluminescent emissions that can be varied from 440 to 500nm (Table 2). For example, UCR-18GaS-AEP can be excited by a broad spectral range from 300 to 470nm (lex-max= 375nm) and emits at 500nm (FWHM ≈ 100nm) and UCR-5ZnGaS has a strong emission at 440nm when excited at a slightly shorter wavelength (368nm).

Gallium sulfide superlattices reported here are more thermally stable than corresponding indium sulfides. UCR-7GaS-TETA was selected to examine zeolitic properties of these new materials. After heating at 280°C in flowing argon, over 49% of H and 63% of N were removed. The XRD shows no deterioration in the sample crystallinity. UCR-7GaS-TETA remained crystalline after being heated at 300°C in air while UCR-7InS-AEP was found amorphous under the same condition.

Templated Assembly of Sulfide Nanoclusters into Cubic-C_3N_4 Type Framework

We have also prepared a series of compounds (collectively denoted as UCR-8) that possesses a type of framework topology never previously observed in open framework solids (Table 3). UCR-8 can be synthesized in more than one chemical composition from a non-aqueous solvent by employing different divalent metal ions such as Fe^{2+}, Co^{2+}, Zn^{2+} and Cd^{2+}. In UCR-8, the inter-cluster S^{2-} atom simultaneously bridges three supertetrahedral clusters to form a rare (3, 4)-connected three-dimensional framework with alternating 4-connected corner-less T4 clusters ($M_4In_{16}S_{31}$, M = Fe, Co, Zn, and Cd) and 3-connected sulfur atoms. Prior to this work, a sulfur atom has not been known to bridge more than two supertetrahedral clusters

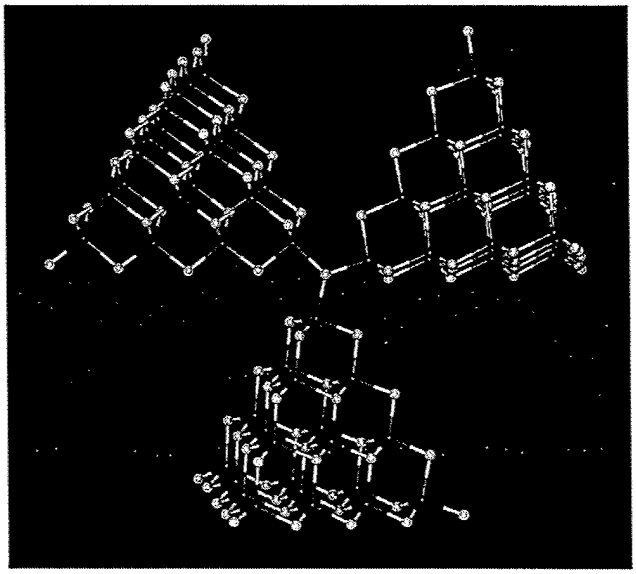

Fig. 5 Three T4 clusters are joined together by a tri-coordinated sulfur.

(T2 or larger). In a (3,4)-connected framework, the ratio of tetrahedral clusters to trigonal atoms is inversely proportional to their connectivity (i.e., 3:4). Therefore, the overall formula of the framework is $(Zn_4In_{16}S_{31})_3(S)_4$ that can also be written as $(Zn_{12}In_{48}S_{97})^{26-}$.

UCR-8 has a framework topological type identical to that of the theoretically calculated cubic carbon nitride (cubic-C_3N_4) with S substituting for trigonally coordinated N atoms and $Zn_4In_{16}S_{31}$ substituting for tetrahedral carbon atoms (Fig. 5). The core of the $M_4In_{16}S_{31}$ cluster, a tetrahedrally coordinated sulfur atom, occupies the same position as the C atom in the cubic C_3N_4. The coordination environment of the 3-connected vertex (i.e. S^{2-}) is quite planar and has an In-S-In angle of 117.0°. The In-S-In angles in UCR-8 range from 104.1 to 117.0 degree and the formation of the cubic C_3N_4 type framework in UCR-8 seems related to the relative flexibility of the In-S-In angle, particularly, the ability to form an angle closer to 120 degree.

Compared to the C-N distance of 1.46 Å in the cubic-C_3N_4 phase, the distance from the 3-connected vertex to the 4-connected vertex in UCR-8 is increased by over 6 times to 9.51Å (cubic unit cell lengths: 5.40Å for cubic-C_3N_4 and ≈35.0Å for UCR-8). The average dimension of six edges of the T4 cluster measured between corner metal atoms is 11.5Å. The large size of the T4 supertetrahedron leads to a large extra-framework space that is about 62% of the crystal volume as calculated with the program PLATON. This extra-framework space is occupied by highly disordered and charge-balancing organic guest molecules. UCR-8ZnInS-DBA has also been found to exhibit a strong photoluminescent emission (FWHM ≈ 100nm) centered at about 470nm when excited at 410nm.

III. The plan of current and future uses of the instrument:

The Bruker D8 Advance thete/theta X-ray Diffracometer with high temperature (up to 1,600°C) attachment and solid-state detector has been installed at our site. Because a demonstration model was available at the time of purchase, we were able to include in our purchase a high temperature attachment and a humidity sensor, which make it possible to study powder diffraction under controlled temperature and environment. The initial service training by the manufacturer's technical staff has been completed. The installed instrument is under the supervision of PI and one graduate student Nanfeng Zheng. Dr. Xianhui Bu is also available for technical consulting and help. New users are first trained by our radiation safety officers on the safe and proper use of x-ray radiation and users must pass a written examination before they can have the access to the x-ray diffractometer.

The first-year instrument operation is under Bruker's warranty. The users are currently charged with $15.00 per hour. The income from the recharge is completely used towards the maintenance cost of the instrument. The recharge rate will be regularly evaluated and adjusted on the basis of the maintenance cost. It is anticipated that the instrument will continued to be greatly appreciated and fully used by both research groups and educational staff on campus and outside community.

Table 1. A summary of crystallographic data for UCR-20, UCR-21, UCR-22, and UCR-23 structures.

Name*	Framework Composition	Space Group	a(Å)	c(Å)	R(F)	Framework Density
UCR-20GaGeS-AEP	$Ga_xGe_{4-x}S_8$	I-43m	20.9884(17)	20.9884(17)	6.65	5.19
UCR-20GaGeS-TAEA	$Ga_{2.67}Ge_{1.33}S_8$	I-43m	20.9352(15)	20.9352(15)	7.21	5.23
UCR-20GaGeS-BAPP	$Ga_xGe_{4-x}S_8$	I-43m	21.293(2)	21.293(2)	7.11	4.97
UCR-20GaGeS-AEM	$Ga_xGe_{4-x}S_8$	I-43m	21.139(4)	21.139(4)	5.44	5.08
UCR-20GaSnS-TMDP	$Ga_{1.80}Sn_{2.20}S_8$	I-43m	21.5404(17)	21.5404(17)	5.54	4.80
UCR-20 InGeS-TMDP	$In_{3.00}Ge_{1.00}S_8$	I-43m	21.734(2)	21.734(2)	7.61	4.69
UCR-20 InSnS-TMDP	$In_{2.50}Sn_{1.50}S_8$	I-43m	22.1906(18)	22.1906(18)	7.61	4.39
UCR-20GaSnSe-TMDP	$Ga_{2.31}Sn_{1.69}Se_8$	I-43m	22.157(3)	22.157(3)	7.61	4.41
UCR-20GaGeSe-TMDP	$Ga_xGe_{4-x}Se_8$	I-43m	21.893(2)	21.893(2)	7.40	4.57
UCR-20GaGeSe-TEPA	$Ga_xGe_{4-x}Se_8$	I-43m	21.874(2)	21.874(2)	5.59	4.59
UCR-21GaGeS-HMI	$Ga_xGe_{4-x}S_8$	I-42d	11.5128(13)	18.912(3)	6.65	6.38
UCR-21GaGeS-AEP	$Ga_xGe_{4-x}S_8$	I-42d	11.280(2)	19.506(6)	6.54	6.45
UCR-21GaGeS-APM	$Ga_xGe_{4-x}S_8$	I-42d	11.2864(18)	19.214(5)	5.87	6.54
UCR-21GaGeS-AEM	$Ga_xGe_{4-x}S_8$	I-42d	11.599(4)	19.817(11)	6.55	6.00
UCR-21GaGeS-APO	$Ga_{3.3}Ge_{0.7}S_8$	I-42d	11.1414(15)	19.405(4)	4.18	6.64
UCR-21GaGeS-DAP	$Ga_xGe_{4-x}S_8$	I-42d	11.0535(16)	19.540(4)	4.18	6.70
UCR-21GaSnS-TAEA	$Ga_{2.32}Sn_{1.68}S_8$	I-42d	11.6915(19)	19.898(5)	4.46	5.88
UCR-21InGeS-APP	$In_{1.84}Ge_{2.16}S_8$	I-42d	11.5313(15)	19.936(4)	6.96	6.04
UCR-21InGeS-PEHA	$In_{1.92}Ge_{2.08}S_8$	I-42d	11.4416(13)	20.210(3)	5.68	6.05
UCR-21GaSnSe-TAEA	$Ga_{2.47}Sn_{1.53}Se_8$	I-42d	12.5373(19)	20.564(4)	6.04	4.95
UCR-22GaGeS-AEP	$Ga_{3.33}Ge_{0.67}S_8$	I4(1)/acd	22.532(2)	39.954(5)	6.23	6.31
UCR-22GaSnS-AEP	$Ga_{2.13}Sn_{1.87}S_8$	I4(1)/acd	22.935(2)	40.985(6)	5.51	5.94
UCR-22InGeS-AEP	$In_{2.69}Ge_{1.31}S_8$	I4(1)/acd	22.9078(12)	41.490(3)	5.82	5.88
UCR-22InGeS-TETA	$In_{2.39}Ge_{1.61}S_8$	I4(1)/acd	22.737(2)	41.591(6)	7.14	5.95
UCR-22InGeS-TAEA	$In_{2.58}Ge_{1.42}S_8$	I4(1)/acd	22.813(3)	41.331(7)	6.84	5.95
UCR-22GaSnSe-TOTDA	$Ga_{1.73}Sn_{2.27}Se_8$	I4(1)/acd	23.841(3)	42.555(7)	6.83	5.29
UCR-23GaGeS-AEM	$Ga_{2.67}Ge_{1.33}S_8$	I-4	21.638(3)	11.209(2)	5.43	6.10
UCR-23InGeS-AEM	$In_{1.84}Ge_{2.16}S_8$	I-4	22.153(3)	11.3435(18)	6.79	5.75
UCR-23GaSnS-AEM	$Ga_{2.29}Sn_{1.71}S_8$	I-4	22.169(3)	11.3168(18)	5.68	5.75

Crystal structures were solved from single-crystal data collected at 298 K on a SMART CCD diffractometer with MoKa. For UCR-21InGeS-AEM, β=16.035(4)Å, β =129.551(6)° , for UCR-21InSnS-AEP, β=16.943(3)Å.

*AEP=1-(2-aminoethyl)piperazine, $C_6H_{15}N_3$;
TMDP=4,4'-trimethylenedipiperidine, $C_{13}H_{26}N_2$;
TAEA=tris(2-aminoethyl)amine, $C_6H_{18}N_4$;
TETA=triethylenetetramine, $C_6H_{18}N_4$;
BAPP=1,4-bis(3-aminopropyl)piperazine, $C_{10}H_{24}N_4$;
HMI=hexamethyleneimine, $C_6H_{13}N$;
AEM=N-(2-aminoethyl)morpholine, $C_6H_{14}N_2O$;
APM=N-(3-aminopropyl)morpholine, $C_7H_{16}N_2O$;
APO=DL-1- amino-2-propanol, C_3H_9NO;
APP= 1-(3-aminopropyl)-2-pipecoline, $C_9N_2H_{20}$;
DAP=1,2-diaminopropane $C_3H_{10}N_2$;
TOTDA=4,7,10-trioxa-1,13—tridecanediamine, $C_{10}H_{24}N_2O_3$;

PEHA= pentaethylenehaxamine, $C_{10}N_6H_{28}$;
TEPA= tetraethylenepentamine, $C_8N_5H_{23}$

Table 2. A summary of important data for selected structures synthesized in this study.

Name	Framework Composition	Space Group	a (Å)	b(Å)	c (Å)	R(F)	λem	λex
UCR-18GaS-AEP	$[Ga_{10}S_{17.5}(S_3)_{0.5}]^{6-}$	C2/c	35.903(5)	18.501(3)	21.183(3)	6.41	500	375
UCR-19ZnGaS-TETA	$[Ga_{10}S_{18}{\bullet}Zn_4Ga_{16}S_{33}]^{16-}$	$I4_1/a$	21.087(2)	21.087(2)	35.582(6)	6.08		
UCR-5ZnGaS-BAPP	$[Zn_4Ga_{16}S_{33}]^{10-}$	$I4_1/acd$	22.595(3)	22.595(3)	40.905(8)	6.71	440	368
UCR-7GaS-TETA	$[Ga_{10}S_{18}]^{6-}$	$I4_1/acd$	19.201(2)	19.201(2)	29.815(4)	5.85	476	370
UCR-7GaS-TAEA	$[Ga_{10}S_{18}]^{6-}$	$I4_1/acd$	19.220(3)	19.220(3)	29.866(6)	5.80		
UCR-7GaS-DBA	$[Ga_{10}S_{18}]^{6-}$	$P4_12_12$	18.803(4)	18.803(4)	29.591(8)	9.92		
UCR-7GaInS-TETA	$[Ga_{4.5}In_{5.5}S_{18}]^{6-}$	$I4_1/acd$	19.715(2)	19.715(2)	30.996(4)	5.87	457	367
UCR-7InS-AEP	$[In_{10}S_{18}]^{6-}$	$I4_1/acd$	20.318(2)	20.318(2)	31.994(5)	4.74		

(a) For UCR-18GaS-AEP, $\beta = 115.992(3)^\circ$.

Table 3. A summary of crystallographic data for selected UCR-8 structures.

Name	Framework Formula	a (Å)	R(F)	$2\theta_{max}$
UCR-8FeInS-DBA	$(Fe_{12}In_{48}S_{97})^{26-}$	35.090(4)	6.41	40
UCR-8CoInS-DBA	$(Co_{12}In_{48}S_{97})^{26-}$	35.002(3)	6.75	45
UCR-8ZnInS-DBA	$(Zn_{12}In_{48}S_{97})^{26-}$	34.981(4)	6.11	45
UCR-8CdInS-DBA	$(Cd_{12}In_{48}S_{97})^{26-}$	35.194(8)	8.79	32

(a) The space group is I-43d for all compounds.